Channeling Effects in the Energy Loss of 3–11-MeV Protons in Silicon and Germanium Single Crystals*

B. R. APPLETON

Bell Telephone Laboratories, Murray Hill, New Jersey and Rutgers, The State University, New Brunswick, New Jersey

AND

C. ERGINSOY

Brookhaven National Laboratory, Upton, New York

AND

W. M. GIBSON

Bell Telephone Laboratories, Murray Hill, New Jersey and Rutgers, The State University, New Brunswick, New Jersey

(Received 31 March 1967)

Planar and axial channeling effects of 3–11-MeV protons in 25–50-μ-thick silicon and germanium single crystals were investigated by studying the direction and energy distributions of the transmitted particles. The total energy distributions were investigated as a function of crystal orientation using a large-acceptance-angle solid-state detector. Limiting angles of incidence for channeling were obtained at several incident energies and crystal thicknesses. The energy and intensity as a function of emergence angles (for a fixed angle of incidence) were obtained by scanning the emergent proton distributions with a small-acceptance-angle detector ($75.\times10^{-7}$ sr) or a masked lithium-drifted position-sensitive detector in a plane 102 cm from the crystal. The least energy loss for protons transmitted parallel to the ⟨110⟩ and ⟨111⟩ axes and the {111}, {110}, and {100} planes of silicon were investigated, and it was found that the least energy loss for each axis was the same as that of the most open planes intersecting at that axis. Measurements of the least energy loss and its straggling were made for the {111} and {110} planes of silicon and germanium. A mechanism of least energy loss is presented for which it is assumed that the energy loss of the well-channeled protons is due to interactions with the weakly bound valence electrons only. The measurements agree well with the theory and are used to extract the local density of valence electrons sampled by the well-channeled protons. A theoretical model of channeling is presented and comparisons made with experiment. Average potentials for the atom rows and planes of silicon are calculated for the static lattice at different temperatures. Multiple Coulomb scattering into channels is considered, as well as the trajectories of the high-loss particles.

1. INTRODUCTION

THE established theories of the interaction of charged particles with matter[1–3] make no distinction between crystalline and amorphous matter. Experiments carried out in recent years have shown, however, that particles incident at small angles to atomic rows or planes in single crystals exhibit anomalous penetrations[4–7] and energy-loss rates,[6–19] as well as orientation-dependent atomic and nuclear[20–26] reaction yields. These effects are usually referred to as particle "channeling." Related anomalous effects (so-called "blocking") also occur near symmetry directions in a crystal when charged particles are emitted from lattice sites[27–29] or are scat-

* This work has been performed under the auspices of the National Science Foundation (Rutgers, The State University), Bell Telephone Laboratories, and the U. S. Atomic Energy Commission (Brookhaven National Laboratory).

[1] N. Bohr, Mat. Kgl. Danske Videnskab. Selskab., Mat. Fys. Medd. **18**, No. 8 (1948).

[2] H. A. Bethe, Ann. Physik **5**, 325 (1930).

[3] F. Bloch, Ann. Physik **16**, 285 (1933); Z. Physik **81**, 363 (1933).

[4] G. R. Piercy, F. Brown, J. A. Davies, and M. McCargo, Phys. Rev. Letters **10**, 399 (1963).

[5] E. V. Kornelsen, F. Brown, J. A. Davies, B. Domeij, and G. R. Piercy, Phys. Rev. **136**, A1849 (1964), and references therein.

[6] J. A. Davies, L. Eriksson, and P. Jespersgaard, Nucl. Instr. Methods **38**, 245 (1965).

[7] R. S. Nelson and M. W. Thompson, Phil. Mag. **8**, 1677 (1963); **9**, 1069 (1964).

[8] G. Dearnaley, IEEE Trans. Nucl. Sci. **11**, 243 (1964).

[9] T. C. Madden and W. M. Gibson, IEEE Trans. Nucl. Sci. **11**, 254 (1964).

[10] C. Erginsoy, H. E. Wegner, and W. M. Gibson, Phys. Rev. Letters **13**, 530 (1964).

[11] A. R. Sattler and G. Dearnaley, Phys. Rev. Letters **15**, 59 (1965).

[12] S. Datz, T. S. Noggle, and C. D. Moak, Phys. Rev. Letters **15**, 254 (1965).

[13] S. Datz, T. S. Noggle, and C. D. Moak, Nucl. Instr. Methods **38**, 221 (1965).

[14] H. E. Wegner, C. Erginsoy, and W. M. Gibson, IEEE Trans. Nucl. Sci. **12**, 240 (1965).

[15] W. M. Gibson, C. Erginsoy, H. E. Wegner, and B. R. Appleton, Phys. Rev. Letters **15**, 357 (1965).

[16] B. R. Appleton, C. Erginsoy, H. E. Wegner, and W. M. Gibson, Phys. Letters **19**, 185 (1965).

[17] B. W. Farmery, R. S. Nelson, R. Sizmann, and M. W. Thompson, Nucl. Instr. Methods **38**, 231 (1965).

[18] B. R. Appleton, M. Altman, L. C. Feldman, E. J. Ludwig, W. M. Gibson, and C. Erginsoy, Bull. Am. Phys. Soc. **11**, 176 (1966).

[19] H. O. Lutz, S. Datz, C. D. Moak, and T. S. Noggle, Phys. Rev. Letters **17**, 285 (1966).

[20] W. Brandt, J. M. Khan, D. L. Potter, R. D. Worley, and H. P. Smith, Jr., Phys. Rev. Letters **14**, 42 (1965).

[21] M. W. Thompson, Phys. Rev. Letters **13**, 756 (1964).

[22] E. Bøgh, J. A. Davies, and K. D. Nielsen, Phys. Letters **12**, 129 (1965).

[23] E. Bøgh and E. Uggerhøj, Phys. Letters **17**, 116 (1965).

[24] E. Bøgh and E. Uggerhøj, Nucl. Instr. Methods **38**, 216 (1965).

[25] J. U. Anderson, J. A. Davies, and K. O. Nielsen, Nucl. Instr. Methods **38**, 207 (1965).

[26] L. C. Feldman, Ph.D. thesis, Rutgers, The State University, 1967 (unpublished).

[27] B. Domeij and K. Björkvist, Phys. Letters **14**, 127 (1965).

[28] B. Domeij, Nucl. Instr. Methods **38**, 207 (1965).

[29] G. Astner, I. Bergström, B. Domeij, L. Erikson, and A. Persson, Phys. Letters **14**, 308 (1965).

tered to large angles by the lattice atoms.[26,30–33] The investigations reported in this paper are a systematic study of the "channeling" phenomenon by the energy loss of 3–11-MeV protons transmitted through single crystals of silicon and germanium.

The energy loss of charged particles of MeV energies in matter is determined by the inelastic collisions, while the trajectories of the particles are determined by deflection in the screened Coulomb fields of the nuclei.[1] For interactions with atomic electrons, as well as with the nuclei, the probability for the basic event to occur is high only when the particle comes sufficiently close to an atom or nucleus. In an amorphous solid, the impact parameters of successive collisions suffered by the particle are *randomly* distributed and the total yield of a reaction over a given path length is independent of the direction along which the particle moves. However, in a crysralline solid atoms are regularly arranged in rows and in planes. Under certain conditions the impact parameters of successive collisions may become *correlated* and their distribution is not random. Hence, the yield of the same reaction for a given path length of the particle may strongly depend on direction. For example, trajectories confined to regions between atomic planes will sample a lower electron density than the average and therefore will experience a lower energy loss than normal, while some trajectories penetrating deeply into the atomic planes will sample a higher electron density than the average, and therefore yield an energy loss larger than normal.

When the particle moves at a small angle to an atomic row or plane, its trajectory is governed by successive correlated small-angle deflections from a large number of lattice atoms. These deflections tend to confine the particle to the open "channels" between the atomic planes or rows. The motion can, therefore, be treated in terms of an average potential[7,34,35] $\bar{V}(\rho)$ in the transverse plane normal to the trajectory.

A particle of mass M and energy E, making an angle ψ with a channel axis, has a transverse momentum $(2ME)^{1/2}\psi$ and the criterion for stable channeling may be written as

$$E\psi^2 \leq \bar{V}(\rho_{\min}) \tag{1}$$

or

$$\psi \leq \psi_c, \quad \text{where} \quad \psi_c = (\bar{V}(\rho_{\min})/E)^{1/2}, \tag{2}$$

and where $\rho_{\min}$ is the distance of closest approach to a row of atoms.

In Sec. 2 the experimental apparatus is discussed and the types of measurements which were made are outlined. The results of these measurements are presented in Sec. 3. Section 4 contains the theoretical calculations and comparisons with experiment. Concluding remarks are made in Sec. 5.

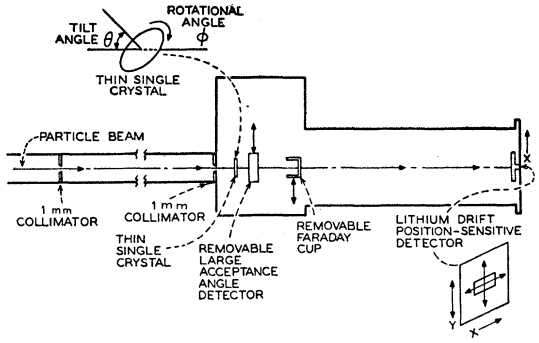

FIG. 1. Experimental apparatus.

2. EXPERIMENTAL

The experimental apparatus used in these experiments is shown schematically in Fig. 1 and is conveniently divided into three main parts for descriptive purposes: (a) a collimating system for defining the proton beam divergence, position, and direction; (b) a goniometer for controlling the crystal orientation relative to the incident beam direction; (c) a system of charged-particle detectors and their associated instrumentation for measuring the energy, intensity, and angular distribution of the transmitted protons. The essential details of these three parts are discussed below.

A. Beam Collimating System

The incident proton beam, produced and accelerated in the Rutgers University—Bell Telephone Laboratory Tandem Van de Graaff, was collimated by annular collimators of various sizes and distances of separation. The minimum collimator size used was 1-mm diameter since it was found that smaller sizes caused proton scattering from the collimator edges. In addition, magnetic focusing and antiscattering collimators were used to minimize collimator edge scattering from the beam handling system. The angular divergence and profile of the proton beam transmitted through the collimating system was investigated in some cases by scanning the beam at a distance of 1 m from the last collimator with a small acceptance-angle detector. The measured full angle of divergence agreed very well with that calculated from the collimator geometry and there was no evidence of appreciable collimator edge scattering. The full angle of divergence of the proton beam varied from 0.17° to 0.03° and is noted with each corresponding measurement.

B. Crystal Specifications and Orientation

Single crystals of silicon and germanium 2 cm in diameter and of various thicknesses between 30 and

[30] D. S. Gemmell and R. E. Holland, Phys. Rev. Letters **14**, 945 (1965).
[31] A. F. Tulinov, Dokl. Akad. Nauk SSSR **162**, 546 (1965) [English transl: Soviet Phys.—Doklady **10**, 463 (1965)].
[32] A. F. Tulinov, B. G. Akhmetova, A. A. Puzanov, and A. A. Bednyakov, JETP Pis'ma. Redaktsiya, **2**, No. 1, 48 (1965) [English transl.: JETP Letters **2**, 30 (1965)].
[33] A. F. Tulinov, V. S. Kulikauskas, and M. M. Malov, Phys. Letters **18**, 304 (1965).
[34] J. Lindhard, Phys. Letters **12**, 126 (1964); Kgl. Danske Videnskab. Selskab., Mat. Fys. Medd. **34**, No. 14 (1965).
[35] C. Erginsoy, Phys. Rev. Letters **15**, 360 (1965).

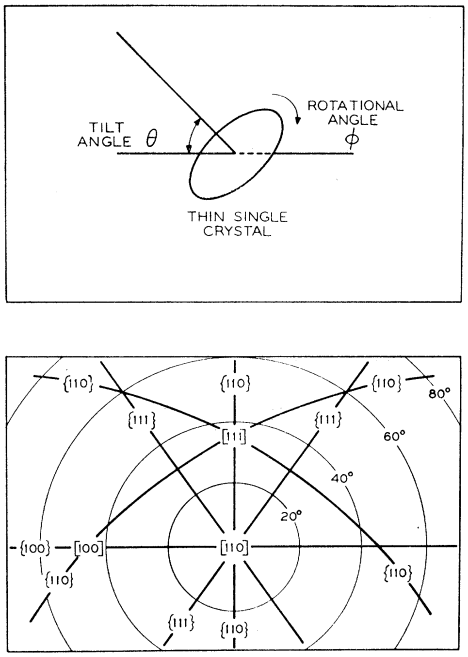

FIG. 2. (a) Tilt (θ) and rotational (ϕ) angles available with the goniometer for orienting the single crystals relative to the incident beam. (b) Stereographic projection of the planes and axes of a diamond-type lattice centered on the ⟨110⟩ axial direction. The planes and axes shown are those investigated in silicon and germanium.

50 μ were used. The thin crystals were cut from vacuum zone-refined crystals of high resistivity and long carrier lifetime, mechanically lapped and polished, and chemically etched to their final thickness by the planar etching technique described by Madden and Gibson.[36,37] In each case a layer of at least 100 μ was etched from each surface to ensure removal of structural damage due to cutting and polishing operations. The crystal thicknesses were initially determined from thickness gauge measurements which indicated their nonuniformity to be less than 1% and some were checked by x-ray transmission measurement.[38] In all cases accurate thicknesses were derived from the energy loss of protons transmitted in a random direction in the crystals (see Sec. 3).

The crystals were clamped gently in the center of the goniometer where they could be tilted by an angle θ and rotated in the plane of the crystal by an angle φ. These angles are indicated in Fig. 1 and Fig. 2(a). The manner in which different crystal directions could be aligned with the incident beam by changing the angles θ and φ can be seen from the diagram in Fig. 2(b). This figure shows a stereographic projection of the low-index planes and axes of a diamond-type lattice centered on the ⟨110⟩ axial direction. Different points on this stereogram correspond to different directions of incidence of the particle beam on a silicon or germanium crystal having its ⟨110⟩ axis at $\theta=0$ as the tilt angle θ and the rotational angle φ are varied. Beam directions corresponding to a fixed value of θ describe a circle centered on the ⟨110⟩ axis, while φ defines the position on this circle. With this arrangement the crystal thickness offered to the beam does not change with φ for a given θ and it is possible to investigate directional effects over a wide range of angles. When the crystal is tilted by an angle θ and rotated around the normal axis by an angle $\Delta\varphi$, the beam direction changes by an angle $\Delta\Psi$ given by the relation

$$\Delta\Psi=\Delta\varphi\sin\theta. \quad (3)$$

This is shown in Fig. 3. Therefore, when θ is small the change $\Delta\Psi$ can be smaller than the change $\Delta\varphi$. For example, at $\theta=5°$, for a rotational change of 0.1°, the actual change of the crystal orientation with respect to beam is $\Delta\Psi=0.01°$.

The θ and φ adjustments on the goniometer could be made with a precision of $\pm0.1°$ by direct reading of vernier scales.

C. Experimental Arrangements

1. Wide Acceptance Angle Measurements

Measurements of this type were made by placing a large solid-state detector directly behind the crystal. The active area of this detector was sufficiently large to accept essentially all the particles transmitted through the crystal. In this way it was possible to study the energy-loss characteristics of the transmitted protons as a function of their incidence angles in the crystals.

The large detector produces a signal pulse height which is proportional to the energy of the transmitted proton. This signal was amplified by a charge-sensitive preamplifier and linear amplifier, and the pulse-height distribution, or energy spectrum, was then stored in a

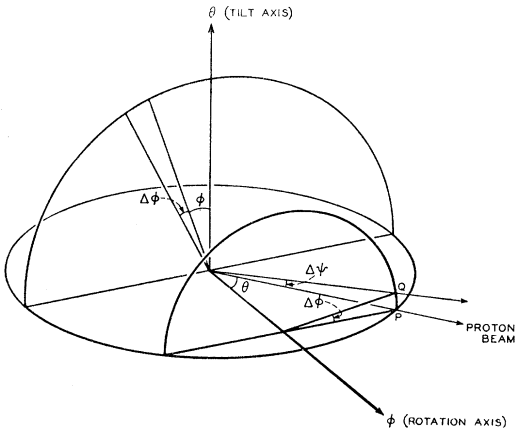

FIG. 3. Sterogram model showing the change in actual internal angle of the beam direction in a crystal lattice ($\Delta\psi$) resulting from a change in ϕ, ($\Delta\phi$), for a fixed θ.

[36] T. C. Madden and W. M. Gibson, Bull. Am. Phys. Soc. 9, 493 (1964).
[37] T. C. Madden and W. M. Gibson, IEEE Trans. Nucl. Sci. 11, 254 (1964).
[38] We are indebted to Dr. K. T. Keating of Brookhaven National Laboratory for carrying out the x-ray measurements.

400-channel pulse-height analyzer or in an on-line SDS-910 computer programmed as a 512-channel pulse-height analyzer.

The energy spectra of the transmitted protons were measured for different beam directions and for different incident proton energies and crystal thicknesses. The results of such measurements are reported in Sec. 3 A.

2. *Energy and Angular-Distribution Measurements of Emerging Particles*

These measurements were designed to determine the scattering patterns of protons emerging from the thin single crystals and to investigate correlations between the scattering distributions and energy loss. As Fig. 1 illustrates, a remote x-y drive on the end of an extension attached to the goniometer chamber made it possible to position a particle detector in the plane perpendicular to the incident beam direction at 102 cm from the crystal. For a fixed angle of incidence the energy and intensity distribution of the emerging particles were studied as a function of their angles of emergence.

Some measurements were made using a small surface-barrier detector with a 1-mm-diam aperture, while others were made with a lithium-drifted position-sensitive detector. The small counter measurements were recorded in the same manner described for the large-acceptance-angle measurements of Sec. 2 A. The energy and incidence positions of protons entering the position-sensitive detector can be simultaneously obtained by means of the electronic system represented in the block diagram of Fig. 4. Two charge pulses are received from the position-sensitive detector (PSD) for each incident proton; one proportional to the energy loss of the incident particle (E), and the other proportional to the product of the position of incidence of the particle and the particle energy loss (PEL). These are divided in an analog divider circuit[39] to give a pulse height proportional to P. Then the pulses proportional to position and energy are analyzed and stored in the SDS-910 computer programmed as a 4096-channel two-dimensional pulse-height analyzer.

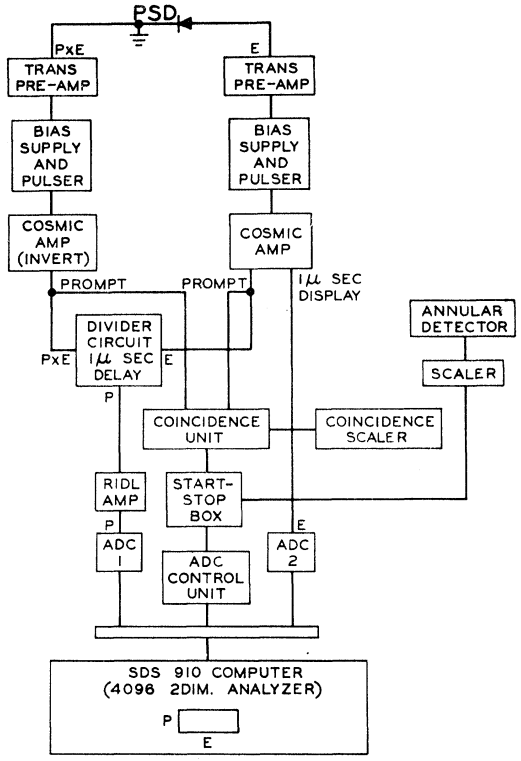

FIG. 4. Position-sensitive-detector electronics diagram.

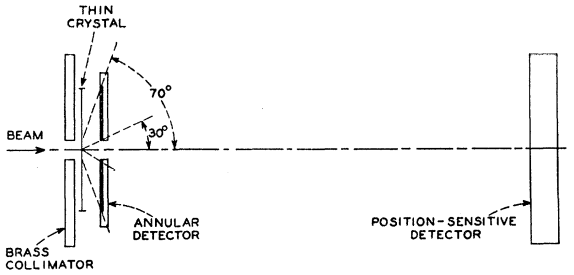

FIG. 5. Annular detector arrangement used to normalize various position-sensitive-detector measurements to the same number of incident particles on the thin crystal.

The fabrication of the position-sensitive detectors, which had 2-mm to 3-mm sensitive thicknesses, has been described by Ludwig.[40] The multiparameter use of the computer is described more completely elsewhere.[41,42]

Measurements of the emerging protons were often needed at various x–y locations for the same number of incident particles on the crystal. In order to normalize such measurements without interfering with the emerging particles of interest, a solid-state detector in the form of an annular ring was used. A diagram of the annular detector as it was utilized is shown in Fig. 5. An annular brass collimator placed in front of the silicon crystal shielded the annular detector from particles that might be scattered from the beam collimators. The detector was placed behind the crystal to intercept protons scattered from the crystal at angles between 30° and 70°. For a fixed beam direction the number of protons scattered to wide angles is proportional to the number of incident protons and the scattered beam can be used to normalize different runs.

3. RESULTS

A. Energy Spectra of Transmitted Particles

The energy loss was studied as a function of crystal orientation by tilting the crystal by an angle $\theta = 10°$ and rotating it about the $\langle 110 \rangle$ axis. The large acceptance

[39] E. A. Gere and G. L. Miller, IEEE Trans. Nucl. Sci. **10**, 382 (1964).
[40] E. J. Ludwig, Rev. Sci. Instr. **36**, 1175 (1965).
[41] J. V. Kane, in Proceedings of the Conference on the Utilization of Multiparameter Analyzers in Nuclear Physics, Sec. 6, 6.2, and 149, (unpublished).
[42] J. V. Kane and R. J. Spinrad, Nucl. Instr. Methods **25**, 141 (1963).

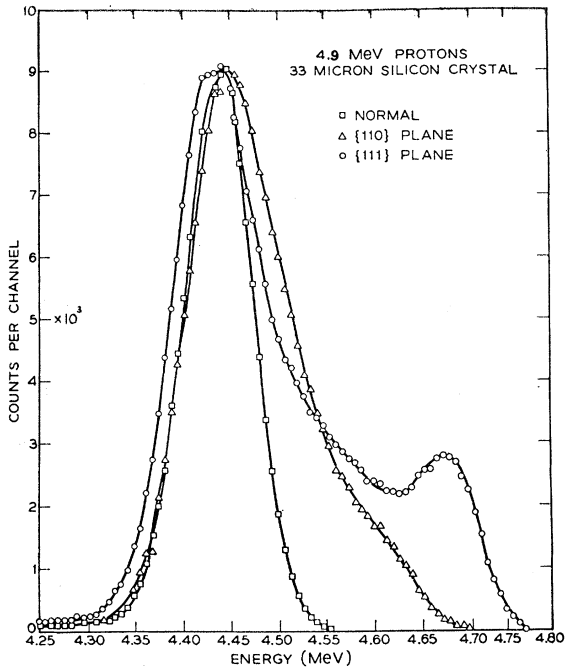

FIG. 6. Transmitted-energy spectra, normalized to the same peak height, for 4.9-MeV protons incident parallel to the {111}, {110} planes, and in a random direction of a 33-μ-thick silicon crystal.

angle detector, Fig. 1, was placed directly behind the crystal. The different spectra for an incident proton energy of 4.9 MeV are shown in Fig. 6. The curve labeled "normal" was obtained for the protons incident in a direction far from any low-index planes or axes in the crystal. This so-called random direction gives an energy-loss spectrum equivalent to that expected for an amorphous silicon sample of the same thickness. We shall refer to the energy loss of particles in this case of the misoriented crystal as the "normal" energy loss. The maximum incident-beam divergence in these measurements was 0.06° at full width. The spectra for incidence parallel to the {110} and {111} planes indicate that a large fraction of the particles are transmitted with lower energy loss than normal. This feature is particularly pronounced when the beam is incident parallel to the {111} plane. In addition, there is also evidence from Fig. 6 that some particles have lost more energy than normal. These two effects will be discussed in Sec. 4.

The spectra of particles transmitted parallel to the same crystal planes are also sensitive to the energy of the incident proton beam, as shown in Fig. 7. These spectra show the energy lost in a 33-μ-thick silicon single crystal by 2.8-, 7.0-, and 11-MeV protons incident parallel to the {111} plane.

The fraction of low-loss particles is considerably larger when incidence is parallel to a low-index axis instead of a plane. This can be seen from Fig. 8, which shows an energy spectrum for 9.0-MeV protons transmitted parallel to the ⟨110⟩ axis of a 48-μ-thick silicon crystal and recorded in the large detector placed behind the crystal. The incident-beam divergence was 0.03° to 0.06° full angle. Also shown for comparison is a normal energy spectrum taken at the same crystal thickness and energy, but with the beam incident in a random direction in the crystal. A large fraction (~0.80) of all the particles transmitted have a lower than normal energy loss. The relative importance of axial and planar channeling for these crystal thicknesses and proton energies was briefly treated in a previous letter[16]; this problem will be discussed in more detail in Sec. 3 B.

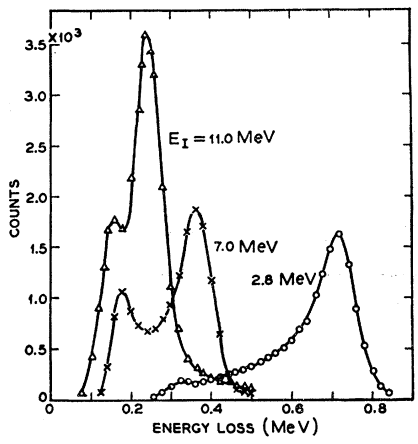

FIG. 7. Energy-loss spectra for 2.8-, 7.0-, and 11.0-MeV protons transmitted parallel to the {111} planes of a 33-μ-thick silicon single crystal. The spectra are plotted for equal areas.

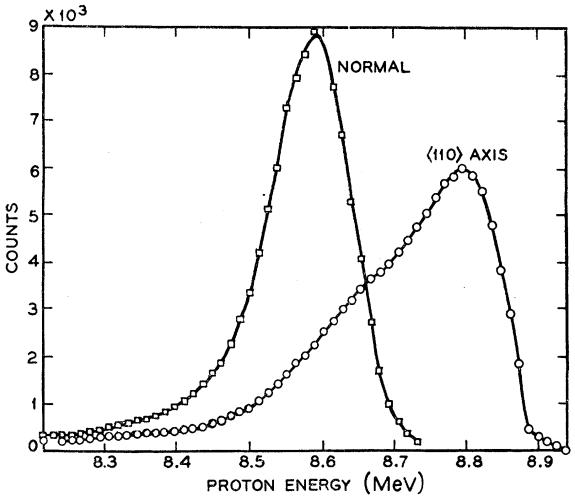

FIG. 8. Transmitted-energy spectra for 9.0-MeV protons transmitted parallel to the ⟨110⟩ axis and in a random direction of a 48-μ-thick silicon crystal. The spectra are plotted for the same number of transmitted protons.

Channeling effects in germanium were also investigated and some of the results are shown in the next two figures. Figure 9 shows three spectra taken with the large-acceptance-angle detector for 9.0-MeV protons

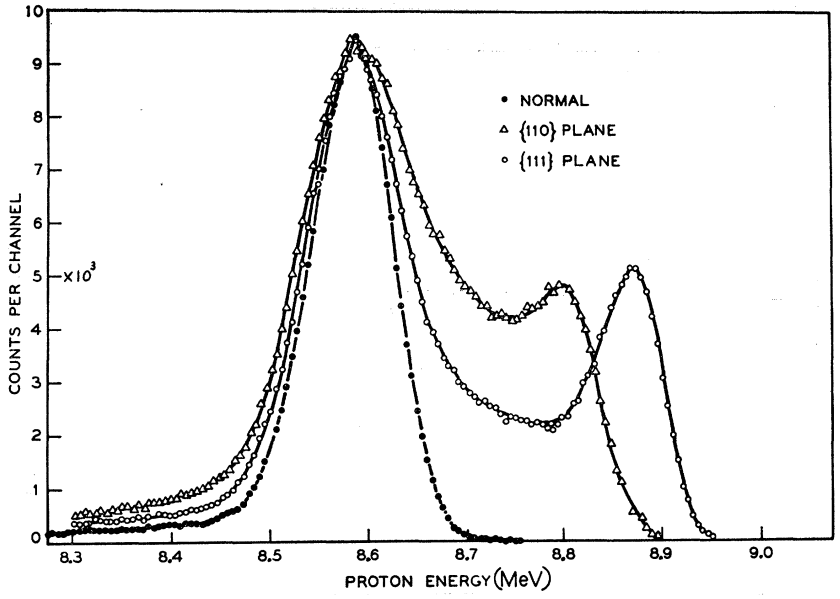

FIG. 9. Transmitted-energy spectra for 9.0-MeV protons incident parallel to the {111}, {110} planes and in a normal direction of a 25-μ-thick germanium single crystal.

incident parallel to the {110} and the {111} planes of a 25-μ-thick germanium crystal. The spectrum for a random direction of incidence is also shown. Figure 10 compares the energy lost by 3.0-, 7.0-, and 11.0-MeV protons in traversing a 25-μ-thick germanium crystal parallel to the {111} plane.

B. Planar and Axial Channeling Effects

It has been shown[16] that planar channeling effects exist independently of any axial channeling in a lattice. There is evidence to suggest that quite apart from this, planar channeling effects are of importance even when the narrowly collimated beam of particles is incident along a crystal axis.[43] Particles wandering from one axial channel to another without changing their azimuthal angle must necessarily sample electron densities that are characteristic of the different planar channels rather than the substantially lower electron density

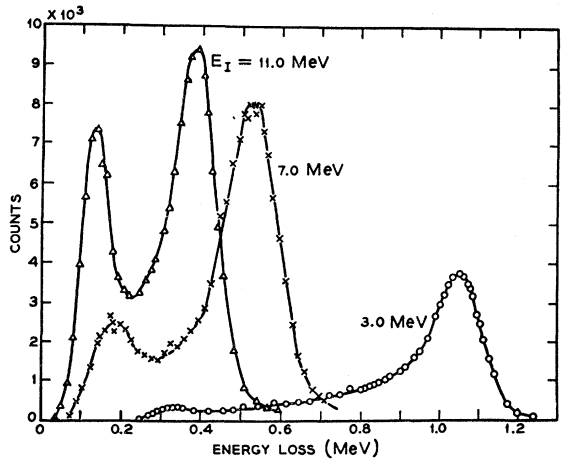

FIG. 10. Energy-loss spectra for 3.0-, 7.0-, and 11.0-MeV protons transmitted parallel to the {111} planes of a 25-μ-thick germanium single crystal. The spectra are plotted for equal areas.

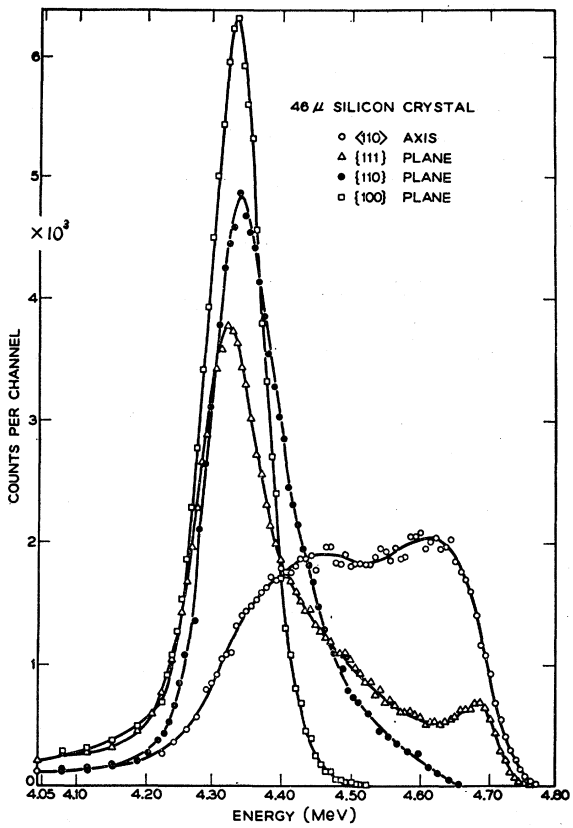

FIG. 11. Energy spectra of 5.0-MeV protons transmitted parallel to the ⟨110⟩ axis, {111}, {110}, and {100} type planes of a 46-μ-thick silicon crystal. The spectra are plotted for equal areas.

[43] B. R. Appleton, W. L. Brown, L. C. Feldman, C. Erginsoy, M. Altman, and J. K. Hirvonen, Bull. Am. Phys. Soc. **12**, 391 (1967).

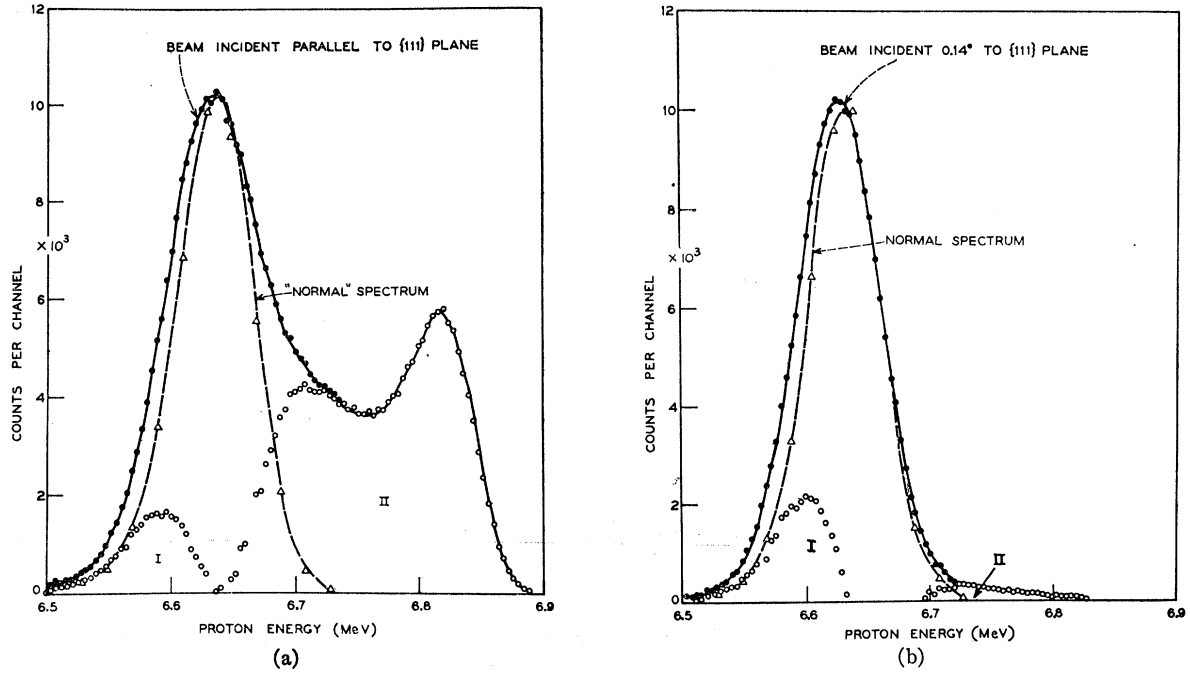

FIG. 12. Energy spectra for 7.0-MeV protons transmitted (a) parallel to the {111} planes, and (b) 0.14° to the {111} planes of a 33-μ-thick silicon single crystal. The dashed energy spectra are for incidence in a random direction and the difference spectra, labeled I and II, were obtained by the subtraction technique outlined in the text.

along a particular axial channel. One can test this interpretation by comparing the energy lost by protons transmitted parallel to an axis with that for protons transmitted parallel to the planes which intersect to form that axis. If some of the protons incident along the axis sample the lower-electron-density characteristics of a particular axial channel, then they should emerge from the crystal with a higher energy than those for any of the planes. Figure 11 shows the transmitted energy spectra for 5.0-MeV protons incident parallel to the ⟨110⟩ axis and the {111}, {110}, and {100} type planes of a 46-μ-thick silicon crystal. Note that the high-energy edge of the ⟨110⟩ axial spectrum coincides with that of the {111} planar spectrum. The same result was found to be true at 7.0 and 9.0 MeV. This indicates that the least energy loss for the ⟨110⟩ axis is the same as that for the most open contributing plane, the {111}, and that few, if any, particles sample a substantially lower electron density. The least energy loss was also the same for the ⟨111⟩ axis and the {110} type planes in a 50-μ-thick silicon crystal at 5 and 7 MeV, as well as for a 10-μ-thick silicon crystal at 5 MeV. However, it is possible that at low energies and for thin crystals particles may be *contained* in a particular axial channel and therefore exhibit smaller energy loss than for any of the planes.[44] A thorough analysis of axial channeling which included various axes and crystal thicknesses has been reported[43] and will be presented in a future paper.

[44] F. H. Eisen, Phys. Letters **23**, 401 (1966).

C. Effect of Incidence Angle

We have seen that protons which undergo channeling are characterized by their anomalously low energy-loss rates. By investigating the fraction of the total beam that suffers energy losses lower than normal, as a function of incidence angle, one can derive the limiting critical angle of incidence for channeling Ψ_c as outlined in the Introduction. The dependence of the high-loss fraction on incidence angle can also be investigated in the same way. These two components of the incidence beam behave anomalously, but result from essentially different mechanisms (Sec. 4).

It is possible to distinguish the two components by their abnormal energy. However, since there are also particles behaving normally and emerging with energies in the normal region, it is necessary to account for this normal fraction and subtract their contribution from the measured spectrum. A lower limit to the anomalous fraction can be obtained by assuming that only normal particles emerge with energies in the normal region and that they have a normal energy distribution. With this assumption, the two anomalous fractions can be estimated by subtracting the normal spectrum (obtained with incidence in a random direction) from the channeled particle spectrum, both spectra being normalized at the peak energy of the normal spectrum. Figures 12(a) and 12(b) show two spectra where this separation has been made. These spectra were recorded by the large-acceptance-angle detector for 7.0-MeV protons incident parallel and at 0.14° to the {111} planes of a 33-μ silicon crystal. The normal spectra are also shown

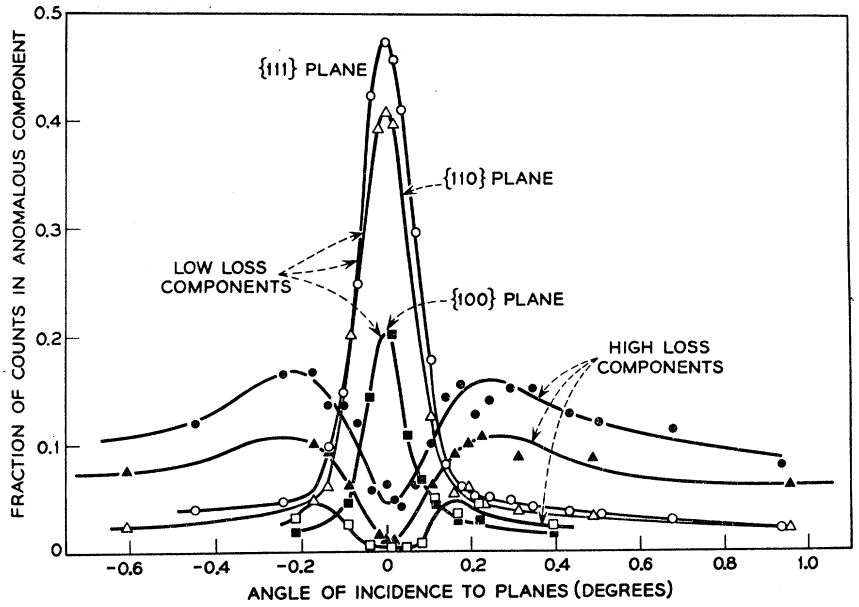

FIG. 13. Fraction of high-loss and low-loss particles in the transmitted-energy distributions as a function of the incidence angle for 2.8-MeV protons relative to the {111}, {110}, and {100} planes of a 33-μ-thick silicon single crystal.

on each figure. The high-loss and the low-loss fractions are given by the areas I and II, respectively, divided by the total area under the spectrum. These parameters will be used in what follows as a measure of the transmitted beam intensity for the two types of anomalous energy loss.

The dependence of these high-loss and low-loss components on incidence angle was investigated for the {111}, {110}, and {100} planes of silicon at several energies and crystal thicknesses. Results are shown in Fig. 13 for 2.8-MeV protons incident with a full angle of divergence of 0.06° on a 33-μ-thick silicon crystal.

A number of features of this angular distribution are of interest: (1) The intensities of the anomalous energy-loss components for the different planes appear to be related to the planar spacing and atomic density in the planes. Both the high-loss and low-loss components are largest for the widely spaced and dense {111} planes, and least for the most closely spaced and least dense {100} planes. (2) The low-loss component drops rapidly as the angle of incidence increases to about 0.14°, where it starts to decrease more slowly. The rapid decrease is consistent with the idea of a critical angle of incidence Ψ_c inside of which particles can be confined by the average planar potential and outside of which they cease to be confined. The presence of low-loss particles for incidence angles outside this critical angle (greater than 0.14°) are believed to be due to initially "normal" particles which were fed into the planar channels by multiple Coulomb scattering. The slow decrease at larger angles is in good agreement with the expected decrease in multiple Coulomb scattering through the indicated angle (Sec. 4). (3) The high-loss component for each of the planes is a minimum at 0°, increases to a maximum for incidence of about 0.2° from the planes, and then decreases slowly at larger angles, again at a rate consistent with multiple Coulomb scattering. (4) The angular widths of the rapidly decreasing portion of the low-loss component distributions are greater than the divergence of the incident beam, so that these widths provide a test of the limiting incidence angles for planar channeling as shown in Sec. 4.

The half-widths taken at the base of the rapidly

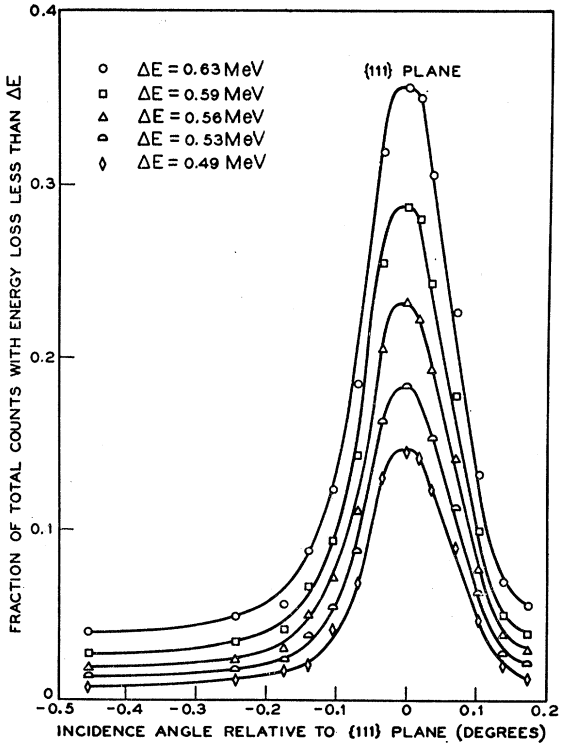

FIG. 14. Fraction of the total particles which emerge with energy loss less than ΔE as a function of the angle of incidence of 2.8-MeV protons relative to the {111} plane of a 33-μ-silicon crystal for various ΔE's.

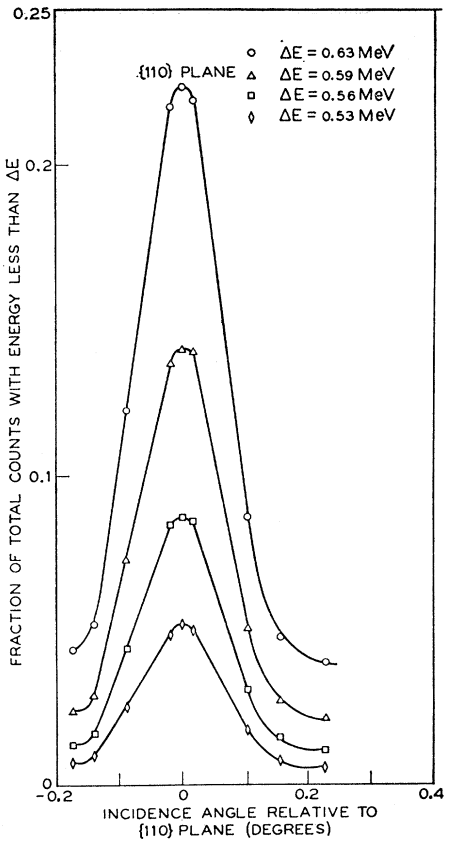

FIG. 15. Fraction of the total particles which emerge with energy loss less than ΔE as a function of the angle of incidence of 2.8-MeV protons relative to the {110} plane of a 33-μ silicon crystal for various ΔE's.

decreasing portion of the low-loss distribution in Fig. 13 are representative of the limiting incidence angle Ψ_c for channeling.

It is possible to adopt an alternative method for estimating Ψ_c from the measured spectra. In Fig. 14 the fraction of the total particles which emerge with energy loss less than ΔE is plotted as a function of incidence angle to the {111} plane for different values of ΔE. The data used are the same as before. Figure 15 shows similar distributions for the {110} planes. For a given plane, the widths obtained in this manner are identical for all ΔE's small compared to the normal energy loss. Also, these widths agree well with those obtained by using the subtraction technique.

In order to test the dependence of Ψ_c on energy, ($\Psi_c \propto 1/\sqrt{E}$), measurements were made with incident proton energies from 2.8 to 8.8 MeV on 33- and 48-μ-thick silicon single crystals. Table I lists the limiting angles of incidence extracted from these measurements for the {111} and {110} planes. These are compared to the calculated widths in Sec. 4.

D. Direction and Energy Correlation of Emerging Particles

Measurements of the energy and intensity distribution of the emerging particles were made using a lithium-drifted position-sensitive detector (PSD) as described in Sec. 2C in conjunction with the on-line SDS-910 computer programmed as a two-dimensional pulse-height analyzer.

The PSD was mounted on the x–y drive illustrated in Fig. 1, at a distance of 102 cm from the crystal. With the beam incident at the desired angle relative to the crystal lattice, the pattern of the emergent particles was scanned with the PSD, which was covered by a mask with eight 1-mm holes, spaced 3 mm apart. The detector could be moved vertically or horizontally with the x–y drive in 1.0-mm steps, thus covering any desired position. A typical measurement, then, would be equivalent to eight separate measurements taken with a small-acceptance-angle solid-state detector. The counts recorded in each hole yield the intensity of protons at that position, as well as the energy distribution.

Such a measurement is illustrated in Fig. 16 for 4.9-MeV protons incident parallel to the {111} plane of a 33-μ-thick silicon single crystal. The insert shows the energy distribution of all the emerging protons independent of their angle of emergence. The masked PSD was normal to the incident beam direction and the {111} planes. Each 1-mm hole of the mask subtends a solid angle of 7.5×10^{-7} sr.

It can be seen that the spectrum at the extreme right, taken at an emergence angle of 3.0°, has an essentially "normal" Gaussian shape and peaks at the normal energy marked by an arrow labeled E_N. However, at $\epsilon=0°$, corresponding to particles emerging parallel to the {111} plane, the spectrum peaks at a higher energy and shows an almost complete absence of particles with normal energy loss. At intermediate emergence angles the intensity of this sharp peak decreases, the peak broadens, and its position shifts to lower energies. Also, a second peak appears at the normal energy E_N. This shows, then, that the low-loss particles emerge predominantly at small angles to the {111} plane. In Table II the peak energy E_c is shown as a function of emergence angle.

The intensity distribution of the emerging particles can be obtained from position-sensitive detector measurements by plotting the total number of counts recorded for each 1-mm hole as a function of emergence angle. Also, the dependence of the anomalous-energy-loss particles on emergence angle can be obtained by analysis of the energy spectra obtained at each angle. Figure 17 shows a comparison of the intensities for a

TABLE I. Measured limiting angles of incidence for the {111} and {110} planes of 33- and 48-μ-thick silicon crystals.

E_I (MeV)	$2\Psi_c$ {111} (measured)	$2\Psi_c$ {110} (measured)	Crystal thickness
2.8	0.28°	0.29°	
4.8	0.22°	...	
			33 μ
6.8	0.17°	0.19°	
8.8	0.16°	0.18°	
5.0	0.21°	0.20°	48 μ

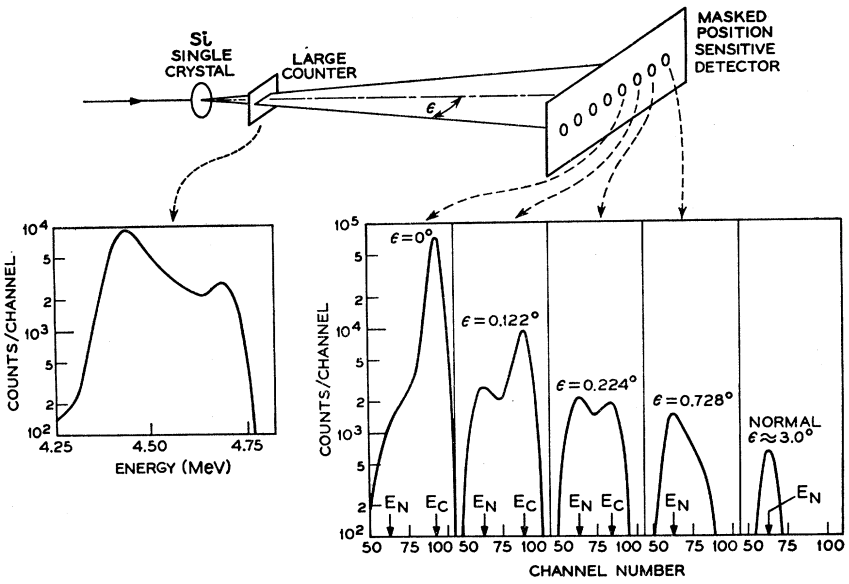

FIG. 16. Illustration of a typical measurement of the emerging proton energy and intensity distribution using a masked position sensitive detector. Shown are the total-energy distribution for 4.9-MeV protons transmitted parallel to the 01110 plane of a 33-μ-thick silicon crystal and the corresponding distributions at various angles of emergence relative to the planar direction within an acceptance angle of 7.5×10^{-7} sr.

"random" incidence and incidence parallel to the {111} plane, in the case of 7.0-MeV protons transmitted through a 48-μ silicon crystal. For this measurement the masked PSD was placed in the direction of the incident beam at 102 cm from the crystal and spectra were recorded in steps of 0.056° of emergence angle. The data were recorded in the computer as position versus energy in a 32- by 128-channel two-dimensional array.

At large angles of emergence the two distributions have similar Gaussian shapes, indicating that particles emerging at these angles are subject to normal multiple scattering. At small emergence angles, however, the channeled particles provide the sharp peak in intensity.

Figure 18 shows the anomalous energy-loss components plotted as a function of the angle of emergence relative to the {111} plane. The number of counts in the high- and low-loss components was obtained from the energy spectra at a given emergence angle by a similar subtraction technique to that discussed in Sec. 3 C. These anomalous component distributions exhibit several interesting features.

(i) The low-loss component maximizes at 0° and drops off rapidly for increasing emergence angles. At larger angles it decreases more slowly. If the slope of the sharply decreasing portion of the low-loss distribution is extrapolated to zero, one can extract a width analogous to that obtained from the low-loss distributions taken as a function of incidence angle. Correcting for the angle subtended by the counter aperture, this full width is 0.20°. The sharp decrease of the low-loss component is consistent with the idea of low-energy-loss particles emerging with a well-defined angular cone of emergence of half-width approximately given by the critical angle ψ_c and the measured angles agree well with the values of ψ_c obtained for incidence measurements (Sec. 3C). The more slowly decreasing wings of the distribution, on the other hand, are probably due to particles which have been channeled for part of their trajectory but escape the channels and then become subject to multiple scattering.

(ii) The magnitude of the high-loss component over the angles investigated is very small compared to that of the low-loss component. However, when all the particles emerging from the crystal are detected (Sec. 3C) the high-loss particles contribute almost 15%. Therefore, the high-loss component must have a much

TABLE II. Peak energy E_c versus angle of emergence relative to the {111} plane for 4.9 MeV protons incident parallel to the {111} plane of a 33-μ-thick silicon single crystal.

E_c (MeV)	ϵ (deg)
4.68	0
4.65	0.056
4.64	0.11
4.61	0.22
4.60	0.28

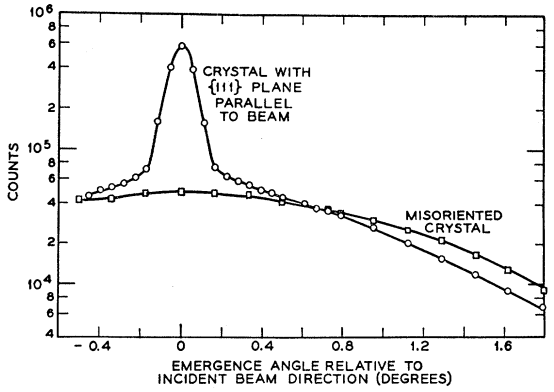

FIG. 17. Comparison, for the same number of incident protons, of intensity as a function of emergence angle for 7.0-MeV protons transmitted parallel to the {111} planes and in a random direction of a 48-μ-thick silicon crystal.

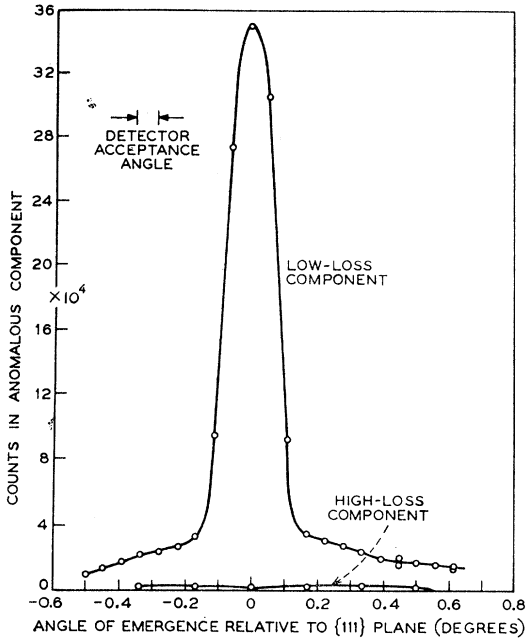

FIG. 18. High-loss and low-loss protons as a function of emergence angle for 7.0 new protons incident parallel to the {111} plane of a 48-μ-thick silicon crystal.

wider angular distribution on emergence than the low-loss component.

E. Least Energy Loss and Straggling

We have seen in previous sections that (1) those particles which lose the least energy when incident parallel to a given crystal plane are those which emerge with the least deflection (Sec. 3D); and (2) that even when the beam was incident parallel to the ⟨110⟩ axis, the least energy loss was the same as for incidence parallel to the {111} plane (Sec. 3B). We have measured the energy loss of these well-channeled particles and the dispersion of the energy loss both in silicon and germanium crystals. The experimental arrangement was similar to that shown in Fig. 1. A small surface-barrier counter with a 1-mm aperture was placed 102 cm from the crystal, and positioned exactly in line with the beam. The crystal was placed in the goniometer and was oriented with the beam parallel to the desired channeling direction. With this crystal orientation and counter position, the small counter then accepted only the least deflected emerging particles, emerging within a solid angle of 7.5×10^{-7} sr.

Figure 19 shows three different energy spectra of the emergent protons as recorded in the small counter for

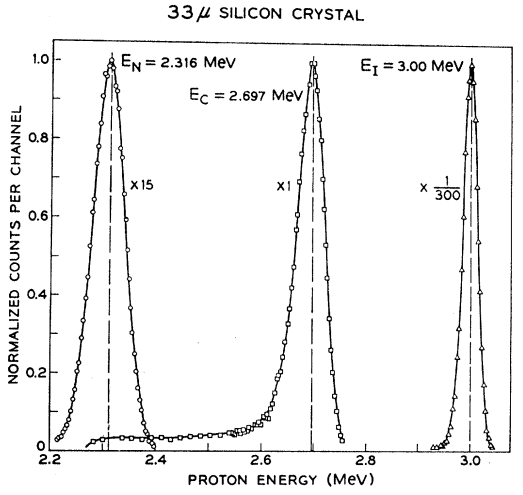

FIG. 19. Energy spectra recorded in a small-acceptance-angle detector (7.5×10^{-7} sr) for 3.0-MeV protons, transmitted in a random direction (left spectrum) and parallel to the {111} planes of a 33-μ-thick silicon crystal (middle spectrum). The incident proton spectrum (at right) was taken with the crystal removed.

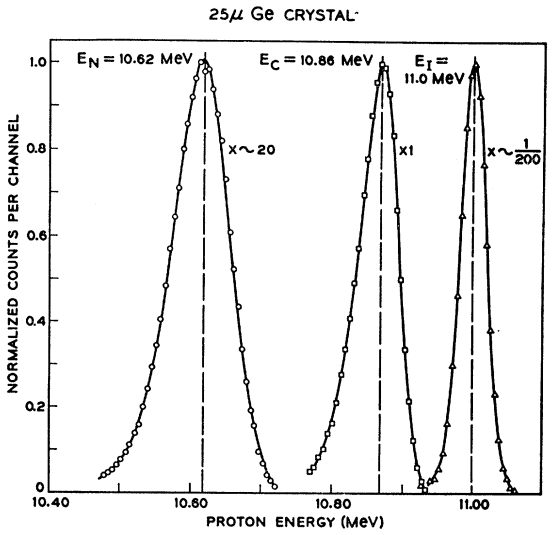

FIG. 20. Energy spectra obtained in the same manner as those in Fig. 19 except for 11.0-MeV protons and a 25-μ-thick germanium crystal.

3.0-MeV protons incident on a 33-μ silicon crystal.

(i) The spectrum on the right refers to the incidence protons and was taken with the crystal removed from the beam. This incident energy is accurately known and was used to calibrate the counter system.

(ii) The middle spectrum was taken with the crystal in place and oriented with the beam incident parallel to the {111} plane.

(iii) The spectrum on the left was taken with the beam incident in a random direction in the crystal but at the same crystal thickness.

The scaling factors beside each spectrum of Fig. 20 indicate the relative magnitudes of these spectra for the same number of incident protons.

It can be seen that the energy loss of the well-channeled protons (E_I-E_C) is about one-half of the normal energy loss (E_I-E_N). This ratio is discussed in Sec. 4E.

Similar measurements were also made for germanium. Figure 20 shows spectra for 11-MeV protons in trans-

TABLE III. Energy loss of channeled and normal protons in silicon crystals.

Crystal	E_I (MeV)	E_C {111} (MeV)	E_C {110} (MeV)	E_N (MeV)	$(E_I-E_C)/(E_I-E_N)$ {111}	$(E_I-E_C)/(E_I-E_N)$ {110}
33-μ Si	2.81	2.49	...	2.08	0.44	...
	2.97	2.68	...	2.28	0.41	...
	3.00	2.70	2.60	2.32	0.44	0.59
	4.43	4.21	4.11	3.94	0.45	0.65
	6.53	6.36	6.29	6.16	0.46	0.65
	7.00	6.84	6.79	6.64	0.43	0.58
	8.58	8.44	8.39	8.27	0.47	0.61
	9.00	8.88	8.82	8.71	0.43	0.62
	11.00	10.90	10.85	10.75	0.42	0.59
48-μ Si	7.00	6.78	...	6.48	0.43	...
	9.03	8.82	...	8.59	0.49	...

mission through a 25-μ-thick Ge crystal. The middle spectrum again refers to the {111} planar channeling.

A tabulation of results with different incident energies and channeling directions is shown in Table III for silicon and in Table IV for germanium.

It can be seen from the spectra in Figs. 19 and 20 that the straggling width of the channeling peak is smaller than that of "normal" particles. The width of the incident spectrum on the right is due to the energy dispersion of the counter system since the incident beam is for all practical purposes monoenergetic. Since the same counter system was used in measuring the other two spectra, their distribution results from a folding of any *real* straggling process and the counter-system dispersion. These two dispersion sources are independent so that they add as the squares. Therefore the *true standard deviations* of the well-channeled and normal spectra can be obtained from their *measured standard deviations* by subtracting out the *measured standard deviation* of the incident-beam spectrum.

The normal spectrum and the incident-beam spectrum have a Gaussian shape, so that one can extract their measured standard deviations by the so-called "probit"[45] method which is illustrated in Fig. 21 for a normal spectrum. By plotting the integral distribution of the Gaussian in the figure one obtains an S-shaped curve with a steepest slope proportional to the reciprocal of the measured standard deviation. The probit method represents a linear transformation of the integrated Gaussian into a straight line, as shown in the figure. This method has the advantage that all the points in the spectrum are used to determine the measured standard deviation allowing a very accurate determination. The standard deviation is given directly by the inverse slope of the probit line.

The energy spectrum of the well-channeled particles of Fig. 19 differs from a Gaussian shape on its low-energy side, because of the presence of particles which have been fed into channels by multiple scattering throughout the crystal and because of the finite acceptance angle of the detector. Therefore, in order to extract the standard deviation due to the least-deflected protons *only*, a Gaussian curve was fitted to the peak and the high-energy side of the spectrum. Such a fit is illustrated in Fig. 22.

A tabulation of the dispersion data for protons from 3.0 to 11.0 MeV for the {111} plane of a 33-μ silicon crystal is given in Table V. The first column on the left gives the incident proton energy, the next three columns give the *measured standard deviation* for the incident, least-deflected, and normal protons, respectively. The probit method was used to extract the Λ_I's and Λ_N's and the Gaussian-fit method just discussed was used to extract the Λ_C's. The true standard deviations Ω_N and Ω_C are shown in the last two columns.

4. THEORETICAL MODEL OF CHANNELING AND DISCUSSION OF RESULTS

A. Average Potentials for Atom Rows and Planes

The motion of charged particles at high energies may be treated by the methods of classical mechanics. The DeBroglie wavelengths are very small (10^{-4}–10^{-5} Å)

TABLE IV. Energy loss of channeled and normal protons in germanium.

Crystal	E_I (MeV)	E_C {111} (MeV)	E_C {110} (MeV)	E_N (MeV)	$(E_I-E_C)/(E_I-E_N)$ {111}	$(E_I-E_C)/(E_I-E_N)$ {110}
25-μ Ge	3.00	2.67	2.52	1.95	0.31	0.45
	5.00	4.78	4.68	4.33	0.33	0.48
	7.00	6.83	6.76	6.47	0.33	0.45
	9.00	8.84	8.79	8.54	0.34	0.46
	11.00	10.86	10.81	10.61	0.33	0.47

[45] R. A. Fisher and F. Yates, *Statistical Tables* (Oliver and Boyd, London, 1938); or D. J. Finney, *Probit Analysis* (Cambridge University Press, New York, 1952).

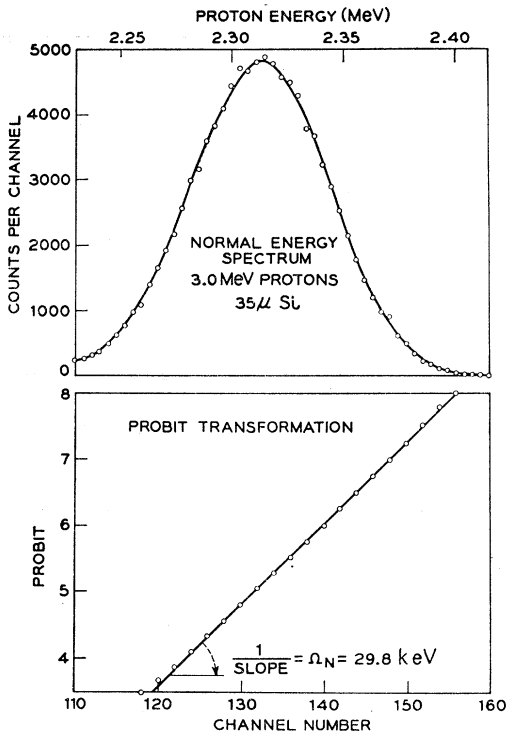

FIG. 21. Representation of the probit-transformation method of obtaining the standard deviation of a Gaussian-shape spectrum. The probit method represents a linear transformation of the integrated Gaussian into a straight line whose inverse slope is the standard deviation.

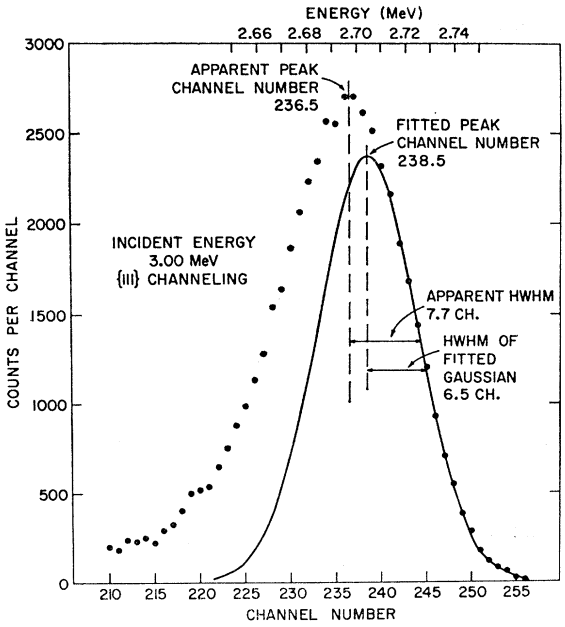

FIG. 22. This figure shows the results of fitting a Gaussian to the peak and high-energy side of a well-channeled energy spectrum to obtain its measured standard deviation.

and the particles move in highly localized wave packets. As far as any coherent scattering or diffraction effects are concerned, inelastic energy losses are so large[46] that no coherence can be said to exist through any finite distance in the crystal.

The trajectory of a particle in the classical sense is always governed by deflections due to atomic fields, even when the energy loss is primarily due to inelastic encounters. The atomic fields are the screened Coulomb fields of the nuclei.

In a "channeling" experiment in which the angle Ψ to an atomic row is very small, some simplifications can be made in estimating deflections. Instead of solving the equations of motion in three dimensions it is possible to make the approximation that the longitudinal component of momentum remains constant. Thus the trajectory of the particle can be projected on a plane perpendicular to the atomic row and the motion of the particle becomes equivalent to the motion of a particle of momentum $Mv\Psi$ or energy $E\Psi^2$ in an average potential due to many atoms. This average potential $\bar{V}(\rho)$ at a distance ρ from the row can be calculated if the potential $V(r)$ between the particle and an individual atom at a separation r is known. For an atomic row with spacing d between atoms, $\bar{V}(\rho)$ is given by

$$\bar{V}(\rho) = \frac{1}{d}\int_{-d/2}^{+d/2} dx\, V(\rho^2+x^2)^{1/2} = \frac{2}{d}\int_0^{\infty} dx\, V(\rho^2+x^2)^{1/2}. \tag{4}$$

As the particle trajectory approaches the atomic row and moves away from it, it comes to a distance of closest approach $\rho_{\min}$ given by the classical relation

$$1-(p^2/\rho_{\min})-[\bar{V}(\rho_{\min})/E\Psi^2]=0, \tag{5}$$

where p is the impact parameter of the "collision" that takes place in the transverse plane upon which the trajectory has been projected.

As an extreme case (giving the lowest value of $\rho_{\min}$ for a given Ψ) we may put $p=0$. This occurs when the trajectory is in the same plane as the row. Equation (5)

TABLE V. Energy widths of incident, least-deflected, and "normal" beams.

E_I (MeV)	Λ_I (keV)	Λ_C {111} (keV)	Λ_N (keV)	$\Omega_N=(\Lambda_N^2-\Lambda_I^2)^{1/2}$	$\Omega_C=(\Lambda_C^2-\Lambda_I^2)^{1/2}$
3.00	14.5	20.2	29.7	25.9	14.1
7.00	15.0	22.5	34.1	30.6	16.8
9.00	16.8	22.6	31.9	27.1	15.2
11.00	16.8	23.6	35.6	31.4	16.6

[46] H. A. Fowler and C. Erginsoy, Phys. Letters **24A**, 390 (1967).

then becomes

$$\bar{V}(\rho_{\min}) = E\Psi^2, \tag{6}$$

or

$$\Psi = [\bar{V}(\rho_{\min})/E]^{1/2}. \tag{7}$$

This relation was first used by Nelson and Thompson[7] in defining the limiting incidence angle if the minimum distance of closest approach $\rho_{\min}$ for stable channeling is known. Lindhard[34] has suggested that $\rho_{\min}$ may be of the order of a_{TF}, the Thomas-Fermi screening radius of the atom.

For an atomic plane there is only one angle Ψ between the trajectory and the plane, and Eq. (7) can be used directly, with $\bar{V}(\rho)$ as the planar average potential given by

$$\bar{V}(\rho) = \frac{2\pi}{A}\int_0^\infty xV(x^2+\rho^2)^{1/2}dx, \tag{8}$$

where $1/A$ is the atomic density in the plane.

As far as $V(r)$ is concerned, several types of screened Coulomb potentials have been proposed.[1,47,48] These are shown in Fig. 23 for the case of a proton and a silicon atom. The unscreened Coulomb potential is given by

$$V(r) = Z_1Z_2e^2/r, \tag{9}$$

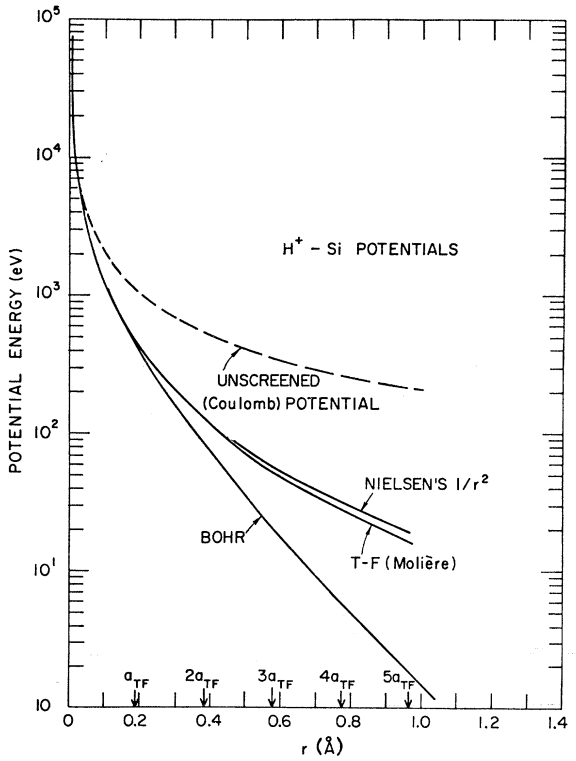

FIG. 23. Interaction potentials between a proton and a silicon atom at different separations. The distance $a_{TF}=0.1943$ Å is the Thomas–Fermi radius of the atom.

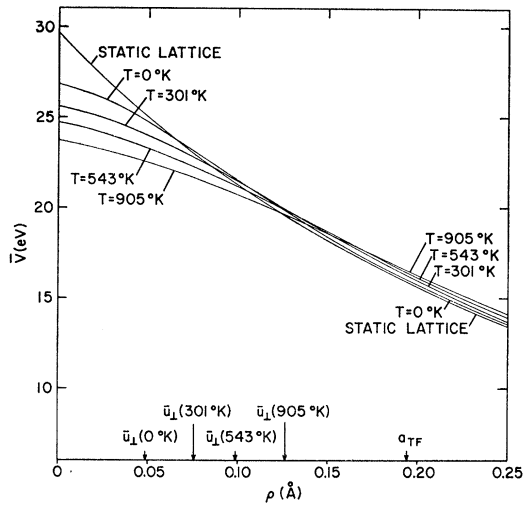

FIG. 24. Average planar potentials for the {111} planes of silicon for the static lattice and at different temperatures. $U_\perp$ represents the rms vibration amplitude normal to the plane.

while Bohr's exponentially screened Coulomb potential is

$$V(r) = (Z_1Z_2e^2/r)\exp(-r/a_B), \tag{10}$$

where $a_B = a_0/(Z_1^{2/3}+Z_2^{2/3})^{1/2}$ is the Bohr screening parameter and $a_0(=0.529$ Å) is the Bohr radius.

It is now generally believed that the Bohr potential gives excessive screening at large separations and that the Thomas-Fermi statistical atom potential might be more appropriate. There is a good analytical approximation to the Thomas-Fermi potential due to Molière.[47] This potential is of the form

$$V(r) = (Z_1Z_2e^2)/r[0.1\exp(-6r/a_{TF})+0.55 \times\exp(-1.2r/a_{TF})+0.35\exp(-0.3r/a_{TF})], \tag{11}$$

where $a_{TF}=0.8853a_0/(Z_1^{2/3}+Z_2^{2/3})^{1/2}$ is the Thomas-Fermi screening radius of the atom.

Another and simpler approximation (but valid only for $r>2a_{TF}$) has been given by Nielsen.[48] This is of the form

$$V(r) = Z_1Z_2e^2a_B/2r^2. \tag{12}$$

Of these different types of screened Coulomb potentials we have chosen the Molière approximation to the Thomas-Fermi potential and have carried out calculations of the average potentials for atomic rows and planes.[35]

The row average potential becomes

$$\bar{V}(\rho) = (2Z_1Z_2e^2/d)[0.1K_0(6\rho/a_{TF})+0.55K_0(1.2\rho/a_{TF}) +0.35K_0(0.3\rho/a_{TF})], \tag{13}$$

where $K_0(x)$ is a zero-order modified Bessel function of the second kind.[49]

The planar average potential for the Molière poten-

[47] G. Moliere, Naturforsch. 2a, 133 (1947).

[48] K. O. Nielsen, *Electromagnetically Enriched Isotopes and Mass Spectrometry* (Academic Press Inc., New York, 1956), p. 68.

[49] G. N. Watson, *Theory of Bessel Functions* (Cambridge University Press, Cambridge, England, 1958), 2nd ed., p. 698.

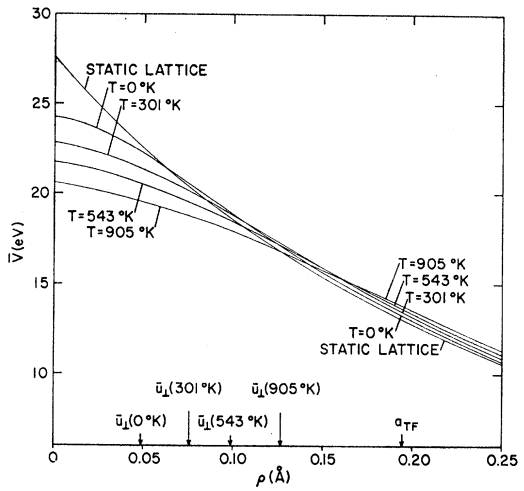

FIG. 25. Average planar potentials for the {110} planes of silicon for the static lattice and at different temperatures. $U_\perp$ represents the rms vibration amplitude normal to the plane.

tial is of the form

$$\bar{V}(\rho)=(2\pi Z_i Z_2 e^2 a_{TF}/A)[(0.1/6)\exp(-6\rho/a_{TF})+(0.55/1.2)\exp(-1.2\rho/a_{TF})+(0.35/0.3)\exp(-0.3\rho/a_{TF})]. \quad (14)$$

B. Effect of Thermal Motion

The above potentials are, of course, for the static lattice and do not take into account the thermal motion of the atoms. The effects of this motion can be easily incorporated in the calculation of average potentials. The plane average potential given by Eq. (14) has three terms, each of which has the general form

$$\bar{V}_i(\rho)=(C_i/A)\exp(-\rho/\alpha_i), \qquad (i=1,2,3). \quad (15)$$

When thermal motion is taken into account, each

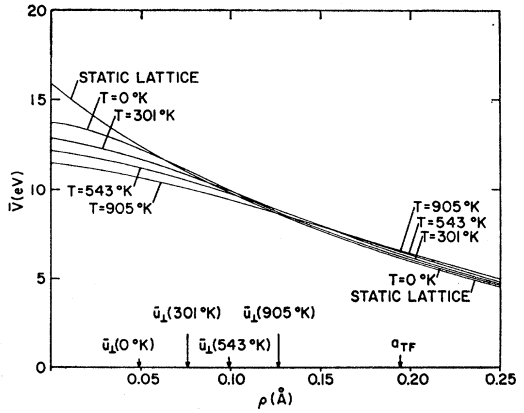

FIG. 26. Average planar potentials for the {100} planes of Si for the static lattice and at different temperatures. $U_\perp$ represents the rms vibration amplitude normal to the plane.

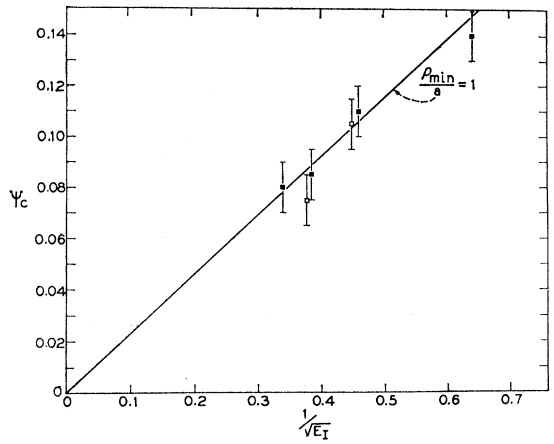

FIG. 27. Experimental limiting angles of incidence as a function of energy (Sec. 3C) compared to calculated values for $\rho_{min}=a_{TF}$ (Sec. 4A). ρ_{min} is the minimum distance of closest approach, a is the Thomas–Fermi screening distance.

atom acquires a probability

$$f(x)=(2\pi u_\perp^2)^{-1/2}\exp(-x^2/2u_\perp^2) \quad (16)$$

of being found at a distance x to the ideal plane. Here u_1^2 is the transverse component of the square of the vibration amplitude.

$$\bar{V}'_i(\rho)=(C_i/A)\left[\int_{-\infty}^{+\infty} dx f(x)\exp(-|\rho-x|/\alpha_i)\right]. \quad (17)$$

The integral in (17) can be carried out explicitly to give

$$\bar{V}_i'(\rho)=\bar{V}_i(\rho)\exp(u_\perp^2/2\alpha_i^2)\times\left\{1-\frac{1}{2}\left[1-\Phi\left(\frac{\rho}{\sqrt{2}u_\perp}-\frac{u_\perp}{\sqrt{2}\alpha_i}\right)\right]+\frac{\exp(2\rho/\alpha_i)}{2}\left[1-\Phi\left(\frac{\rho}{\sqrt{2}u_\perp}+\frac{u_\perp}{\sqrt{2}\alpha_i}\right)\right]\right\}, \quad (18)$$

where

$$\Phi(x)=\frac{2}{\sqrt{\pi}}\int_0^x dt\, e^{-t^2}$$

is the error integral function.[50]

TABLE VI. Calculated average planar potentials (eV) for a proton in the planar channels of silicon (T=301°K).

Plane	$\bar{V}(\rho=0)$	$\bar{V}(\rho=u_\perp)$	$\bar{V}(\rho=a_{TF})$
{111}	25.6	22.7	16.2
{110}	22.8	20.1	13.5
{100}	12.9	10.8	6.3

[50] *Handbook of Mathematical Functions*, edited by M. Abramowitz and I. A. Stegun (U.S. Department of Commerce, National Bureau of Standards, Washington, D.C., 1964), Appl. Math. Ser. 55, Chap. 5, p. 227.

As ρ becomes large we find that $\bar{V}(\rho)$ tends to the limit[50]

$$\bar{V}_i'(\rho)=\bar{V}_i(\rho)\exp(u_\perp^2/2\alpha_i^2), \tag{19}$$

indicating that $\bar{V}_i'(\rho)$ increases slightly with increasing temperature. However, for small ρ the average potential (and therefore the critical incidence angle Ψ_C) decreases with increasing temperature.

We have calculated the effect of temperature on the average planar potentials for different planes of silicon, as shown in Table VI. Figures 24, 25, and 26 show the potential for a proton in the {111}, {110}, and {100} planar channels of silicon. In the case of {111} planes the unequal spacing (alternating 0.78 and 2.35 Å) is taken into account and the potential zero is at the mid-plane of the larger spacing. For other planes the potential is zero at a distance equal to one-half of the planar spacing. It can be seen that the potential decreases substantially below its static-lattice value for small ρ. Table VI gives the values of the calculated potentials at $\rho=0$, $\rho=u_\perp(T=301°\text{K})$, and $\rho=a_{\text{TF}}$. The corresponding critical incidence angles can be easily calculated from Eq. (7).

The distance of closest approach to a plane—and, therefore, the critical incidence angle—is not to be taken as constant for all physical phenomena. For Rutherford scattering, for instance, $\rho=u_\perp$ may be appropriate, while for energy loss $\rho=a_{\text{TF}}$ may be more meaningful.

In Fig. 27 we compare the calculated values $\Psi_C=[\bar{V}(a)/E]^{1/2}$ with the measured widths (Table I in Sec. 3 C). The agreement with the experimental widths is best for $\rho_{\min}\cong a_{\text{TF}}$. The measurement shows the predicted $1/\sqrt{E}$ dependence.

For the axial channeling width we have measured[43] $\Psi_C=0.2°$ for the ⟨110⟩ axis at 5 MeV. The calculated value $\Psi_C=[\bar{V}(a_{\text{TF}})/E]^{1/2}$ is 0.2°.

The average row potential [Eq. (13)] diverges at $\rho=0$ because of the logarithmic divergence of the K_0 function. This is clearly an unrealistic situation since it suggests that atomic rows are impenetrable. However, when the thermal motion of the atoms is taken into account, the potential at $\rho=0$ becomes finite.

Let $f(r)$ be the differential probability that an atom in thermal motion is at a distance r from the ideal "string"

$$f(r)=2r/\langle\sigma^2\rangle\exp(-r^2/\langle\sigma^2\rangle). \tag{20}$$

If the correlation between nearest neighbors is neglected, $\langle\sigma^2\rangle=u_\perp^2=\frac{2}{3}\langle u^2\rangle$, where $\langle u^2\rangle$ is the mean-square thermal-vibration amplitude. The same model could be used with a smaller value of $\langle\sigma^2\rangle$ to represent the effective, or relative, thermal-vibration amplitude when positional correlation has to be taken into account. In the absence of reliable data on the degree of correlation in the case of Si, we shall assume that $\langle\sigma^2\rangle=u_\perp^2$.

The temperature-dependent average potential at

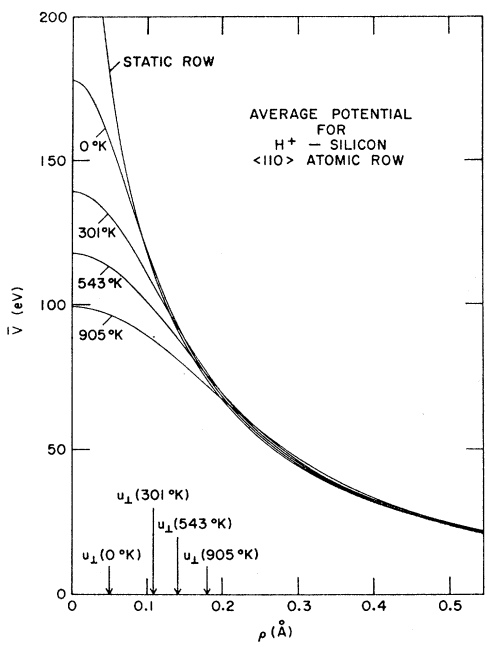

FIG. 28. Temperature-dependent average potentials as a function of distance from the ⟨110⟩ atomic row of silicon. $U_\perp$ represents the rms vibration amplitude normal to the row.

$\rho=0$ can be obtained by integrating

$$\bar{V}_T(0)=\int_0^\infty dr\,f(r)\bar{V}(r). \tag{21}$$

Using [Eq. (13)] this gives

$$\bar{V}_{u_\perp}(0)=(Z_1Z_2e^2/d)[0.1\exp(9u_\perp^2/a_{\text{TF}}^2)E_1(9u_\perp^2/a_{\text{TF}}^2)$$
$$+0.55\exp(0.36u_\perp^2/a_{\text{TF}}^2)E_1(0.36u_\perp^2/a_{\text{TF}}^2)$$
$$+0.35\exp(0.0225u_\perp^2/a_{\text{TF}}^2)E_1(0.0225u_\perp^2/a_{\text{TF}}^2)], \tag{22}$$

where

$$E_1(x)=\int_x^\infty\frac{e^{-z}}{z}dz$$

is the exponential integral function.[50]

Equation (22) shows that $\bar{V}_{u_\perp}(0)$ increases with decreasing $u_\perp$, i.e., decreasing temperature. Such an increase has been observed experimentally.[33,51]

For $\rho>0$ the calculation of the temperature-dependent average potential requires the numerical double integration

$$\bar{V}_T(\rho)=\int_0^\infty dr\int_0^{2\pi}d\theta\,f(r)\bar{V}(\rho^2+r^2-2\rho r\cos\theta).^{1/2} \tag{23}$$

This was done in the case of the ⟨110⟩ atomic row in silicon ($d=3.84$ Å) and Fig. 28 shows the calculated temperature-dependent average potential as a function of distance from the row. It can be seen that at dis-

[51] A. F. Tulinov, Usp. Fiz. Nauk **87**, 585 (1966) [English transl.: Soviet Phys.—Usp, **8**, 864 (1966)].

tances small compared to the thermal-vibration amplitudes of the atoms the average potentials (and, therefore, the angular widths for a given particle energy) decrease more rapidly with increasing temperature than in the case of the planar potentials. At a distance $\rho \approx a_{TF}$, however, the width should be rather insensitive to temperature.

C. Scattering into Channels

Figure 13 in Sec. 3C shows that some particles lose less energy than normal even when the incident beam is at an angle large compared to the critical angle, i.e., when no particles enter the crystal within the acceptance angle of the channeling direction. This suggests that particles are being fed into channels by multiple scattering throughout the crystal.

Consider a well-collimated beam incident on the crystal at an angle Ψ_0 with respect to a planar channel and let 2Δ be the full acceptance angle of the channel. First, we shall obtain an upper limit to the fraction of the beam that suffers a lower energy than normal by neglecting the escape of the particles from the channel. Once a particle is scattered into the channel by small-angle multiple scattering, we shall assume that it maintains its direction within an angle $\pm\Delta$ to the plane throughout the rest of its trajectory. This upper limit is given by

$$p_{\max}(\psi_0, \Delta, t) = 1/(\pi \langle\theta_t^2\rangle)^{1/2} \int_{x_0-\Delta}^{\infty} d\theta_x \exp(-\theta_x^2/\langle\theta_t^2\rangle)$$
$$= \tfrac{1}{2}\{1-\Phi[(\psi_0-\Delta)/(\langle\theta_t^2\rangle)^{1/2}]\}, \qquad (24)$$

where $\langle\theta_t^2\rangle$ is the mean-square scattering angle through a crystal of thickness t and

$$\Phi(x) = \frac{2}{\sqrt{\pi}} \int_0^x dz\, e^{-z^2}$$

is the error integral function.[50] The plane is assumed to lie normal to the x axis.

If particles fed into the channel have a high probability of escape, the channeled fraction reduces to a minimum value given by

$$p_{\min}(\psi_0, \Delta, t) = 1/(\pi \langle\theta_t^2\rangle)^{1/2} \int_{\psi_0-\Delta}^{\psi_0+\Delta} d\theta_x \exp(-\theta_x^2/\langle\theta_t^2\rangle)$$
$$= \tfrac{1}{2}\{\Phi[(\psi_0+\Delta)/(\langle\theta_t^2\rangle)^{1/2}] - \Phi[(\psi_0-\Delta)/(\langle\theta_t^2\rangle)^{1/2}]\}$$
$$\cong 2\Delta \exp[-(\psi_0^2/\langle\theta_t^2\rangle)] \quad \text{for } \Delta \ll \psi_0. \qquad (25)$$

For a given crystal thickness and a given particle energy, $\langle\theta_t^2\rangle$ is fixed. Therefore, when ψ_0 is changed as in the experiments described in Sec. 3 C, $p_{\min}$ varies as $\exp(-\Psi_0^2/\langle\theta^2\rangle_t)$. This should show a Gaussian shape with increasing Ψ_0, which is, in fact, observed (Fig. 13).

D. High-Loss Trajectories

Under optimum channeling conditions, that is, when the angle of incidence with respect to a crystal axis or plane is zero, the fraction of channeled particles in the beam is maximized. However, energy spectra in Figs. 12 and 13 show that under the same conditions, there is a certain number of particles in the beam that suffer a larger energy loss than normal. Obviously these particles are not channeled, since both their emergence pattern (Fig. 18) and their dependence on the incidence angle are different from the channeled particles that suffer a lower energy loss than normal. We have referred to this fraction of the beam in Sec. 3B as the high-loss component. It is necessary to discuss now the possible mechanism that is responsible for high-loss trajectories.

Lindhard[34] has stated some compensation rules according to which, if the crystal thickness is small and there is no appreciable energy change, the yield of a given reaction averaged over all incidence angles must be equal to the yield for the amorphous solid. In other words, energy loss averaged over all incidence angles is equal to "normal" loss and, if there are directions that give a low energy loss compared to normal, there must be others that give a higher loss than normal. Although Lindhard's arguments for the validity of this rule are convincing, the statement of the rule does not answer the basic question regarding the physical mechanism that must be responsible for the existence of a trajectory that samples a consistently high density of electrons so as to experience a higher energy loss than the random path.

The following observations are important in this regard:

(a) The high-loss component is maximized at an incidence angle of 0.2°–0.3° for 3-MeV protons incident on {111} planes. This angle is approximately equal to $\Psi(0) = [\bar{V}(0)/E]^{1/2}$, where $\bar{V}(0)$ is the value of the average planar potential at $\rho = 0$.

(b) For a crystal of the same thickness and at the same proton energy the Rutherford-scattering yield is also maximized at the same incidence angle.[26]

(c) The energy loss suffered by "blocked" trajectories emerging from a single crystal after Rutherford scattering is higher than that of random trajectories following a scattering event of the same angle.[26] The same is true for "blocked" particles directly emitted from lattice sites.[52,53]

These observations are consistent with the model[35]

[52] Measurements made recently at Bell Telephone Laboratories and Rutgers University for protons of MeV energies transmitted through Si.

[53] B. Domeij, Arkiv Fysik **32**, 179 (1966).

TABLE VII. Measured energy loss for channeled particles and estimates by the equipartition rule (Refs. 11, 2).

Crystal	E_I(MeV)	$(\Delta E)_{\{111\}}$	$(\Delta E)_{\text{equip}}$	$(\Delta E)_{\text{equip}}/(\Delta E)_{\text{normal}}$	$(\Delta E)_{\{111\}}/(\Delta E)_{\text{normal}}$
Silicon 1	2.81	0.33	0.35	0.48	0.44
	4.83	0.22	0.24	0.49	0.45
	8.58	0.14	0.15	0.49	0.45
	11.00	0.12	0.12	0.49	0.48
Silicon 2	7.00	0.22	0.25	0.48	0.43
	9.03	0.21	0.21	0.49	0.49
Germanium	5.00	0.22	0.32	0.48	0.33
	7.00	0.17	0.26	0.49	0.32
	9.00	0.15	0.22	0.49	0.33
	11.00	0.12	0.18	0.49	0.33

according to which the high-loss trajectories are essentially those that become subject to the process of "blocking." This mechanism may be looked upon as a case of strong scattering of particles initially moving exactly along an atomic plane or a row with zero average impact parameter. For an isotropic distribution of initial directions, the distribution of emergence directions out of the plane or row is strongly peaked at a certain angle given approximately by $\Psi(0)$. Since energy loss is negligible in this process, the same angle becomes the angle of incidence with respect to the next plane or row. In view of the reversibility of trajectories, it is exactly this angle that, on the average, deflects the particles again *into* the planes or rows. (However, unlike channeled trajectories that are simply reflected by the atomic arrays, the blocked trajectories may emerge from the planes also on the other side.) This process may, therefore, repeat itself while the distribution of emergence angles gets broader and some particles are lost to the random group. There is reason to suppose that the broadening of the distribution makes this mechanism more sensitive to thickness[23,24,33] than channeling, where the potential keeps the particles away from just the same regions where random multiple scattering is strong.

More experimental and theoretical work is required to verify whether the above model is adequate in treating high-loss trajectories and "blocked" trajectories as essentially subject to the same mechanism of scattering. However, the present observations do not give any counterindication in this respect.

E. Role of Valence Electrons in Limiting Least Energy Loss

One of the important questions to which a theoretical model of channeling is required to find an answer is that of the least energy loss of the channeled particles. It has been suggested by Lindhard[34,54] that, on the average, one-half of the stopping power of a fast particle in a system of electrons is due to close collisions (which are minimized by channeling) and one-half to resonance-type distant interactions (which cannot be avoided by channeling). Thus the stopping power of a particle could be reduced by channeling by a factor of 2 at the most.

This prediction by the equipartition rule was believed[10] to be confirmed by early experiments on the energy loss of protons in silicon, but later experiments[11,18] in germanium showed significant disagreements.

Figures 19 and 20 show the spectra of particles transmitted through the crystal in the {111} planar channels of silicon and germanium, respectively, with least deflection (width within a solid angle of 7.45×10^{-7} sr) and compare these spectra with those of the "normal" particles E_N for the same thickness and the incident beam E_I. The spectrum for the "normal" particles is obtained by rotating the crystal away from any low-index plane or axis and that of the incident beam corresponds to the case of no crystal. It can be seen that the channeling peak E_C is almost half-way between the incident energy E_I and the normal emergence energy E_N in the case of silicon; but in germanium E_I-E_C/E_I-E_N is as small as 0.33.

If equipartition held exactly we would expect

$$(-dE/dx)_{\text{dist.}}=(-dE/dx)_{\text{close}}=\tfrac{1}{2}(-dE/dx)_{\text{total}}. \quad (26)$$

The crystal thickness Δx can be expressed as

$$\Delta x=\int_{E_e}^{E_I}\frac{dE}{(-dE/dx)_{\text{total}}}, \quad (27)$$

[54] J. Lindhard and A. Winther, Kgl. Danske Videnskab. Selskab., Mat. Fys. Medd. **34**, No. 4 (1964).

TABLE VIII. Calculated number of effective electrons/atom contributing to channeling loss.

E_I	$Z_{\text{loc}\{111\}}$ (Energy loss)	$Z_{\text{loc}\{111\}}$ (Dispersion)
3.0	3.8	4.1
7.0	4.1	4.1
9.0	4.4	4.4
11.0	4.5	3.9

where E_e is the emerging beam energy. Therefore,

$$\tfrac{1}{2}\Delta x = \int_{E_C}^{E_I} \frac{dE}{(-dE/dx)_{\text{total}}}. \tag{28}$$

In other words, on the basis of equipartition one can estimate the emerging energy of the channeling particles E_C by using normal energy loss but by taking one-half of the crystal thickness.

Table VII shows the measured energy loss $(\Delta E)_{\{111\}} = E_I - E_C$ and the values of $E_I - E_C$ estimated on the basis of equipartition.

It can be seen that agreement with silicon is reasonable, but with germanium (Fig. 20) the energy loss of channeled particles is as small as one-third of the normal. We therefore believe the agreement for silicon to be accidental.

It is useful to look at the energy loss of well-channeled particles on a different basis.[55] As far as core electrons in silicon are concerned, these are in the atomic K and L shells. One can estimate the maximum distance from nuclei at which excitation of such shells are still possible by establishing an adiabaticity criterion

$$\rho_{\max} = \hbar v/\Delta E, \tag{29}$$

where v is the velocity of the particle and ΔE is the binding energy of the electron in its shell.

For a K-shell electron in silicon, $\Delta E = 1845$ eV and $\rho_{\max}$ for a 3-MeV proton becomes as small as 0.05 Å. For well-channeled particles in the {111} planar channels experimental ρ's are of the order of 1 Å. Therefore, K-shell excitation can be neglected.

For L-shell electrons ΔE is between 100 and 150 eV. Taking the value of 100 eV one finds that $\rho_{\max}$ is now about 1.5 Å. Therefore, L-shell excitation cannot be altogether neglected. However, energy loss scales in the ratio

$$\ln\frac{\rho_{\max}}{\rho_{\text{expt}}} \Big/ \ln\frac{2mv^2}{\Delta E}, \tag{30}$$

where $\rho_{\text{expt}} \cong 1.0$ Å for the {111} planes. It follows that the energy loss due to L-shell electrons is reduced by more than 90% by channeling. We shall neglect this loss in what follows.

Energy loss to valence electrons alone can be written in the form

$$(-dE/dx)_{\text{val}} = 4\pi Z^2 e^4 N L/mv^2, \tag{31}$$

where

$$L = Z_{\text{val}} \ln(v/v_F) + Z_{\text{loc}}[\ln(2mvv_F/\hbar\omega p)]. \tag{32}$$

The first term on the right-hand side of (32) corresponds to the contribution of collective (plasma) excitations which use the total density of valence electrons ($Z_{\text{val}} = 4$ in silicon). The second term gives the contribution of the local density of valence electrons in the channels to single-particle excitation. This division of L into two contributions is possible in terms of the random-phase approximation of Bohm and Pines.[56] In the above equation v is the velocity of the particle, v_F the Fermi velocity of the free-electron gas describing the valence electrons, $\hbar\omega_p$ the plasmon energy (16.6 eV in silicon), and $Z_{\text{loc}} = n_{\text{loc}}/N$, where n_{loc} is the local density of valence electrons in the channels.

Knowing the crystal thickness Δx from the measurement of normal energy loss, we can write

$$\Delta x = \int_{E_C}^{E_I} \frac{dE}{(-dE/dx)_{\text{val}}} \tag{33}$$

and obtain Z_{loc} in the different planar channels by integrating Eq. (33) with the use of Eqs. (31) and (32). For the {111} planar channels of silicon and for a proton beam of 3.0 MeV, we obtain $Z_{\text{loc}\{111\}} = 3.8$ by this method.

The straggling of the channeling peak, too, can give information regarding Z_{loc}. Since collective excitations do not cause any appreciable straggling in energy loss [35] the straggling of the well-channeled particles is due to close collisions with the local electrons, and we can write

$$\frac{\Omega_N^2}{\Omega_C^2} = \frac{\Lambda_N^2 - \Lambda_I^2}{\Lambda_C^2 - \Lambda_I^2} = \frac{Z_{\text{total}}}{Z_{\text{loc}}}, \tag{34}$$

where Ω_N^2 and Ω_C^2 are the true variances of the energy loss and channeled loss (Table V).

$Z_{\text{total}} = 14$ in silicon

$\Lambda_N = 29.71$ keV;

$\Lambda_I = 14.50$ keV;

$\Lambda_C = 20.2$ keV;

for $E_I = 3.00$ MeV, as measured (cf. Table V).

This gives $Z_{\text{loc}\{111\}} = 4.1$, which compares well with the $Z_{\text{loc}\{111\}} = 3.8$ estimated by the essentially independent measurement of the energy peaks.

[55] C. Erginsoy, B. R. Appleton, and W. M. Gibson, Bull. Am. Phys. Soc. 11, 176 (1966).

[56] See, for example, D. Pines, *Elementary Excitation in Solids* (W. A. Benjamin, Inc., New York, 1963), p. 148.

At higher energies, losses to L-shell excitation cannot be neglected for channeled particles. However, the results shown below in Table VIII along with the 3.0-MeV result, show reasonable agreement.
It would be valuable to have similar experiments at even lower energies than 3 MeV.

5. CONCLUSIONS

We have made a systematic study of channeling effects in the energy loss of 3–11-MeV protons in silicon and germanium single crystals. The main conclusions of the study may be summarized as follows:

(1) The energy loss is strongly dependent on the direction along which a well-collimated beam of particles enters the crystal. When this direction is parallel to some major crystal axis or plane, a certain fraction of the particles in the beam suffers an energy loss lower than normal. This fraction is largest for the most "open" crystallographic directions. In silicon this is the ⟨110⟩ direction; among planes the {111} planes provide the best channeling.

(2) In addition to the channeled particles that suffer an energy loss that is low compared to the normal loss, there are particles experiencing a larger energy loss than normal. The fraction of such particles in the beam is maximized at an incidence angle where no appreciable channeling occurs. The angular distribution of these high-loss particles is also different from that of channeled particles in emergence from the crystal.

(3) The minimum energy loss associated with the ⟨110⟩ axial channeling is equal, for the same energy and same crystal thickness, to that associated with the {111} planar channeling. The same holds for the ⟨111⟩ axial channeling and {110} planar channeling. This indicates that, over the energy range covered, the well-channeled particles do not stay within an individual axial channel but wander across from channel to channel, sampling an electron density that is essentially equal to that existing between the most widely spaced of the planes that intersect the axis.

(4) The angular widths of channeling agree well with the values calculated on the basis of an average potential, and a distance of closest approach equal to the Thomas-Fermi radius of the atoms.

(5) High-loss trajectories may be looked upon as essentially "blocked" trajectories that are deflected away from atomic planes or rows.

(6) The minimum energy loss suffered by the best channeled particles is well accounted for by the interaction of the particles solely with the valence electrons in silicon, if the energy is sufficiently low that inner-shell electrons do not contribute to excitations at large impact parameters.

ACKNOWLEDGMENTS

We gratefully acknowledge the constant help we have received from our colleagues L. C. Feldman and E. J. Ludwig in the course of this work, as well as several stimulating discussions with W. L. Brown which have helped us in elucidating many points. We also wish to thank T. C. Madden for preparation of the thin single-crystal samples and M. Altman for assistance in the experiments.